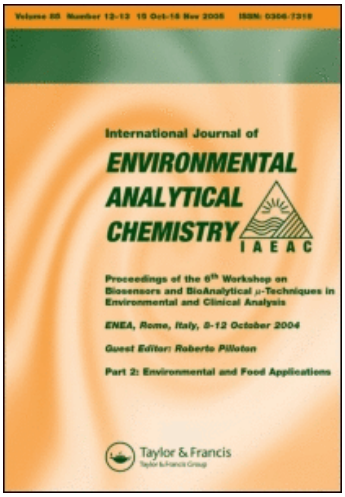

International Journal of Environmental Analytical Chemistry
Publication details, including instructions for authors and subscription information:
http://www.informaworld.com/smpp/title~content=t713640455

Investigation of the Emissions of an Antimony Metallurgical Factory with Transmission Electron Microscopy

P. Bloch[a]; B. Vanderborght[a]; F. Adams[a]; J. Van Landuyt[b]
[a] Department of Chemistry, University of Antwerpen (U.I.A.), Wilrijk, Belgium [b] Centrum voor Hoogspanningselectronenmicroscopie, University of Antwerpen (RUCA), Antwerpen, Belgium

To cite this Article Bloch, P. , Vanderborght, B. , Adams, F. and Van Landuyt, J.(1983) 'Investigation of the Emissions of an Antimony Metallurgical Factory with Transmission Electron Microscopy', International Journal of Environmental Analytical Chemistry, 14: 4, 257 — 274
To link to this Article: DOI: 10.1080/03067318308071624
URL: http://dx.doi.org/10.1080/03067318308071624

Intern. J. Environ. Anal. Chem., 1983, Vol. 14, pp. 257–274
0306-7319/83/1404-0257 $18.50/0

Printed in Great Britain

Investigation of the Emissions of an Antimony Metallurgical Factory with Transmission Electron Microscopy

P. BLOCH, B. VANDERBORGHT, F. ADAMS

Department of Chemistry, University of Antwerpen (U.I.A.), B-2610 Wilrijk, (Belgium)

and

J. VAN LANDUYT

Centrum voor Hoogspanningselectronenmicroscopie, University of Antwerpen (RUCA), B-2020 Antwerpen (Belgium)

(*Received 26 October, 1982*)

Transmission electron microscopy with energy dispersive X-ray fluorescence and selected area electron diffraction has been used for the identification of individual particles in the emissions of an antimony refining plant. Systematic microscopical analysis of 4 distinct Sb-containing particle types can be used to trace sources within the factory and estimate the relative importance of each at distinct sites around the plant. Fugitive emissions appear to be the most important source up to 1.5 km from the factory.

INTRODUCTION

A methodology developed for identification of individual aerosol particles has been reported previously.[1] It is based on transmission electron microscopy at 100 kV, and on electron-induced X-ray analysis and selected area electron diffraction for chemical and structural identification. Sampling of the aerosol is performed directly on Formvar coated electron microscope grids with a 1.0 l min^{-1} Batelle cascade impactor.[2]

In this paper the application of the method to the particulate emissions of an antimony and lead refining plant is described. The factory is situated about 40 km east of Antwerp in a rural environment. The particulate antimony pollution is a specific indicator for the plant and it was selected for a multi-disciplinary air pollution study.[3] Over a period of 14 months simultaneous measurements were performed of the emission rate, the

meteorological conditions, the environmental impact and fall-out of particulate matter at distances of 100 m to 4.2 km downwind from the factory and contamination with Sb in plants and animals. The overall intention of the study was to correlate the measurements with mathematical models for dispersion and deposition.

The objectives of the present microanalytical work consisted in: 1) deriving whether microanalytical methods are able to identify the emission sources within one reasonably complex installation;

2) establishing the link between several emission sources in the factory and the environmental impact at a number of points in the sampling network.

It is clear that these aims require a method which is able to discriminate between particles of roughly the same composition, namely an antimony oxide matrix. On the basis of differences in morphology and dimensions as apparent from the electron microscopical image, the purity of the material from the energy-dispersive X-ray spectra, and the crystallographical structure from electron diffraction, it was estimated that this would be possible. The latter method, although serving a useful purpose for the full characterisation of certain particle categories, cannot be used for routine particle counting purposes however, as it is too time-consuming. As a starting point it is necessary that the various production steps and the fugitive and stack emissions they give rise to, are correlated with the morphology, size, purity and structure of individual particles. Also, it is required that no or at least very minor changes occur in morphology, size and chemical composition between the emission points and the sampling locations.

EXPERIMENTAL

Instrumentation

The particulate material is collected by impaction onto a clean Formvar foil surface. The foils are held onto a transmission electron microscopy (TEM) grid which is placed on the different stages of a 1 l min^{-1} Battelle cascade impactor.[1] On impaction most of the particles are adsorbed onto the Formvar foil but bounce-off of particles cannot be completely neglected. The optimum collection time varies considerably for the different impactor stages, e.g. at a total suspended particulate concentration of 100 $\mu g\,m^{-3}$ between 5 min for stage 5 to 120 min for stage 1. It is defined rather loosely as the time required to collect 100–400

particles per electron microscope grid opening. In some conditions several samples need to be taken and a sample with an appropriate particle density is selected *a posteriori*. After coating with carbon the grids are introduced without any further treatment into the electron microscope for observation and analysis. This eliminates a number of problems associated with sampling through filtration and prevents time-consuming sample preparation procedures. Also, the use of an impactor provides the additional advantage that particles are selected according to their aerodynamic size.

For the observations a Philips EM-300 transmission electron microscope is used at an acceleration potential of 100 kV. The particles encountered in the atmosphere are in most cases sufficiently heat- and radiation-resistant to allow for the normal electron currents used for observation in the transmission and diffraction mode.

Energy dispersive X-ray analysis (EDXRA) is performed with a 10 mm^2 Kevex Si(Li) detector, shielded from the electron microscope vacuum with 7.5 μm Be window. Link Systems amplification and data processing electronics are used. Net peak intensities are obtained through a simple and fast background subtraction procedure at specific energy channels of the spectrum. For complicated spectra, the non-linear least-squares deconvolution program, AXIL (Van Espen *et al.*,)[4,5] is employed. Quantitative analytical data are obtained from the X-ray intensities using the thin film model of Russ *et al.*[6] The model neglects absorption but it was shown that it gives acceptable results on small particles ($<0.3\,\mu$m) and larger thin ones. However, the analytical information should be considered as semi-quantitative. EDXRA can be used in a sufficiently fast way to be an aid in the classification of particles.

Selected area electron diffraction (SAED) is used to derive information concerning the crystal structure. The interplanar spacings of the particle crystal lattice are obtained from the diffraction pattern which consists of a spot array or a ring pattern depending on whether the particle is respectively mono- or polycrystalline or whether several particles are stuck together. The minimum diameter of the selected area is about 2 μm at 100 KeV; the thickness of the sample which gives rise to still measurable SAED patterns is limited to about 50 nm. For internal standardization (determinations of the camera constant) adequate calibration crystals are used whose interplanar distances and indices of the diffraction patterns are well known. To obtain reliable structural information on an unknown particle it is necessary to perform the SAED-measurements several times at different tilt and rotation geometries of the sample. Dark field transmission images are useful for visualizing those parts of the object responsible for particular diffraction spots.

Sampling

The different emission points in the plant are shown in Fig. 1. The sampling points at which fugitive and stack emissions were sampled are marked. The antimony refining process is based on (1) a reduction of the ore with coke to purify antimony metal in the blast furnaces, (2) an oxidation to Sb_2O_3 in the convertors and finally, (3) a purification by reduction with carbon to Sb metal in a refinery oven. There are several of these equipments operational within the factory and one of them (for the convertors 2) was selected for the study.

The stack emissions were sampled downstream from the gas cleaning installations. Stack 1 emits particles from two possible particulate sources, a convertor and a refinery oven. Both emissions were sampled separately (they are marked 1 and 2 for convertor and refinery oven, respectively). Stack 2 which emits particulates from blast furnaces and refinery ovens was also sampled at different intervals of the production process (1 and 2 in the discussion). Stack 3 was sampled when convertor emissions occurred.

Macroscopic amounts of material were also taken from the filter bags of the gas cleaning installations of a convertor and a refinery oven. This material is representative for operation conditions during several weeks. Also, bulk samples were taken at the blast furnace and in each of the stacks.

Sampling in the field was performed downwind from the factory and under stable atmospheric conditions in which the wind direction corresponded within $\pm 5°$ with the axis from the factory to the sampling points which are indicated in Fig. 1. Sampling times of less than 2 min for the stages of the impactor resulted in an adequate loading of the electron microscope grids.[1] Samples were taken simultaneously by remote control of the pumps. With the short sampling time involved it was possible to know accurately which of the process operations were active during sampling.

RESULTS

Antimony-containing particles

The antimony-containing particles emitted in the production process consist exclusively of antimony oxides. Four different crystallographic structures were observed.

1) Senarmontite (cubic Sb_2O_3). These particles appeared to have a different morphological appearance according to the different processes in

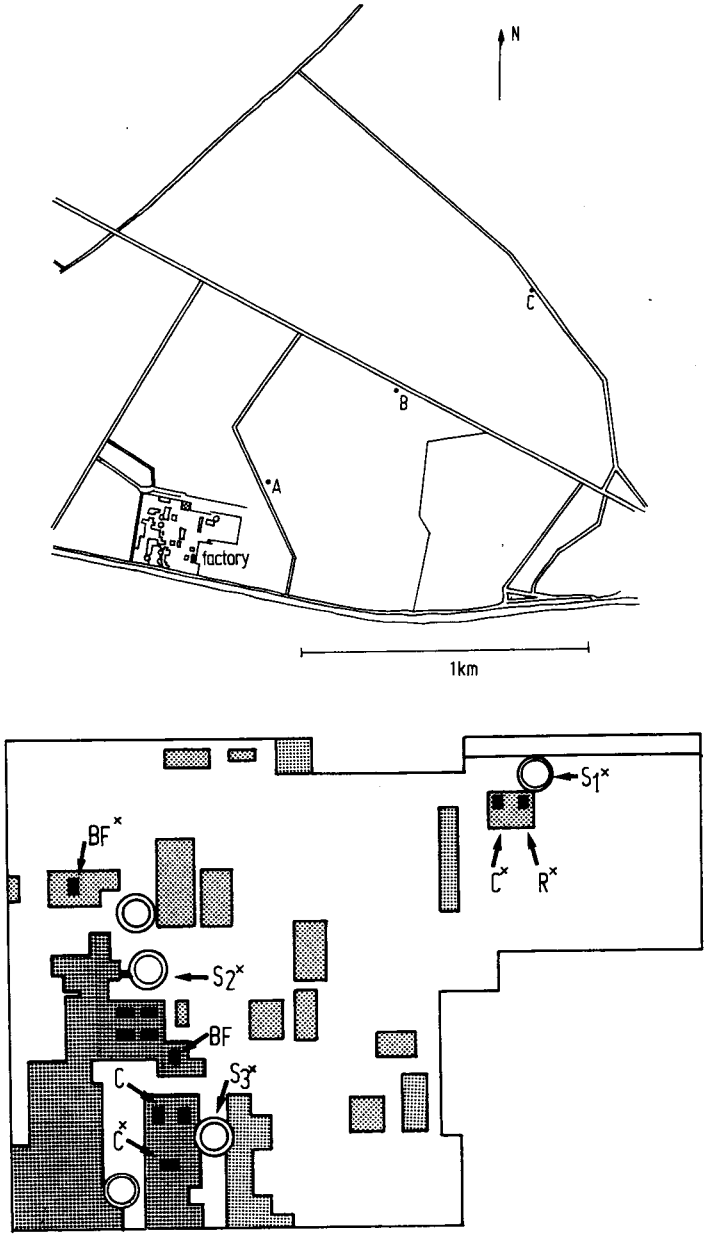

FIGURE 1 Sampling points in relation to the factory and detail of the major emission points (S_1 to S_3: stacks, R: refinery ovens, C: convertors, BF: blast furnace). The dotted areas are buildings. The emission points sampled are marked with an asterisk.

which they are generated: transparent (Fig. 2a) or opaque single (Fig. 2b) crystals or aggregates of small entities.

2) (2, 1):7 superstructure of senarmontite[7,8] (Fig. 2c).

3) Valentinite (orthorhombic Sb_2O_3) needles (Fig. 2d).

4) Spherical particles which usually did not provide a SAED pattern. Exceptionally they did provide a pattern compatible with the cubic Sb_2O_5 structure. It was hence assumed that all these morphologically easily recognisable particles consist of Sb_2O_5. They occur as single particles or as aggregates (Fig. 2c and e).

X-ray powder diffraction (XRD) was utilised for a number of emission samples from which macroscopical amounts of material could be collected. The results indicated the presence of senarmontite, valentinite and crystalline Sb_2O_5. They give further support to the unexpected observation that antimony is emitted in two distinct oxidation states. The superstructure of senarmontite could not be observed with XRD but examination with a high resolution electron microscope at 200 kV gave additional evidence for the presence of this crystallographic structure.

The concentrations of the three detectable varieties obtained by XRD are shown in Table I for material collected at several emission locations. For senarmontite and valentinite standard samples were available for converting the reflex intensities to concentrations. For Sb_2O_5 a theoretical approach was used. As this latter compound is probably overwhelmingly present in an amorphous state, its concentration in Table I must be a serious underestimate.

The antimony factory is also a refining plant for lead and specific emission sources of lead-containing particles were readily detectable. Two

TABLE I

Relative concentration of the crystallographic varieties detected by XRD (weight %).

	Sb_2O_3		
Source	Senarmontite	Valentinite	Sb_2O_5[a]
Blast furnace	85	—	15
Filter bag convertor	91	3	6
Filter bag refinery oven	85	11	4
Stack 1 (convertor)	77	3	20
Stack 1 (refinery oven)	68	10	22
Stack 2	88	—	12
Stack 3	100	—	—

[a]crystalline fraction only.

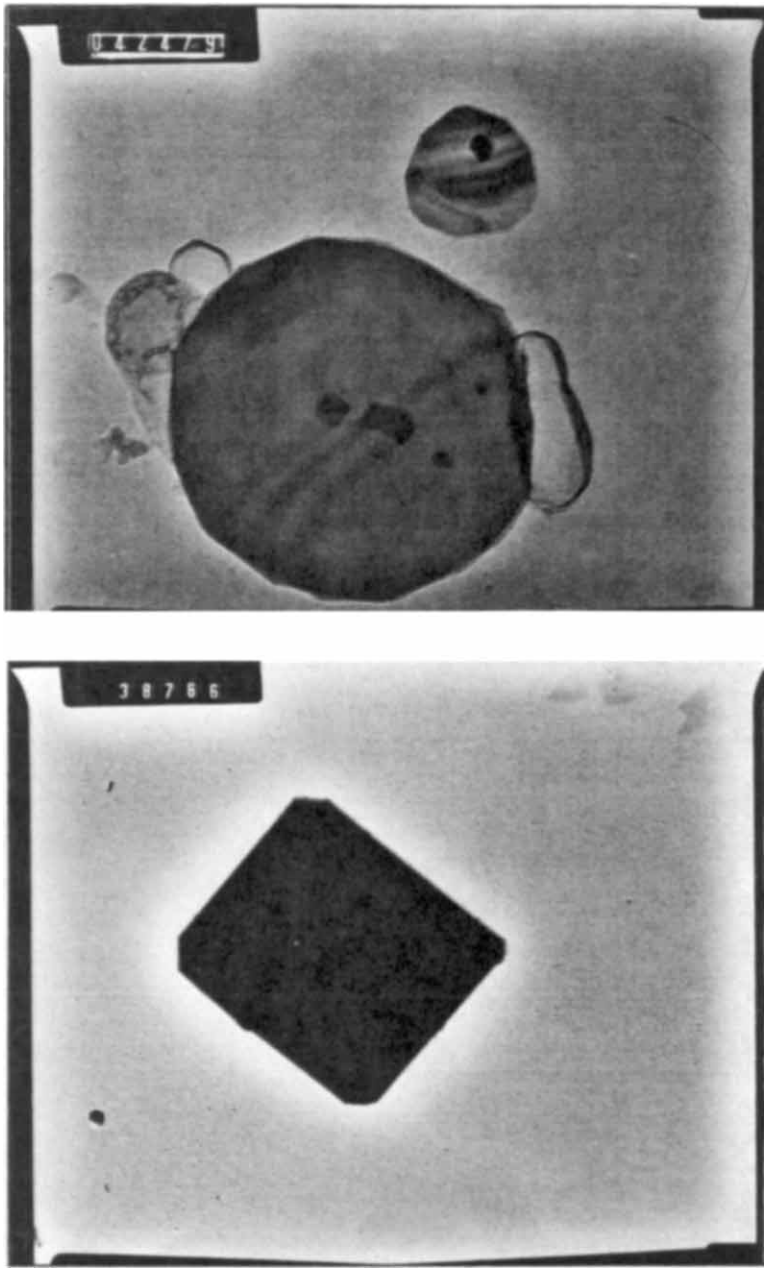

FIGURE 2 TEM-micrographs of some typical antimony containing particles emitted in the Sb-production process. (a) Transparent senarmontite (cubic Sb_2O_3); (b) senarmontite, opaque; (c) (2, 1):7 superstructure of senarmontite and spherical Sb_2O_5 particles; (d) valentinite (orthorhombic Sb_2O_3) and spherical Sb_2O_5 particle; (e) Sb_2O_5 condensation aerosol aggregate; (f) senarmontite (Sb_2O_3) + Sb_2O_5 aggregate.

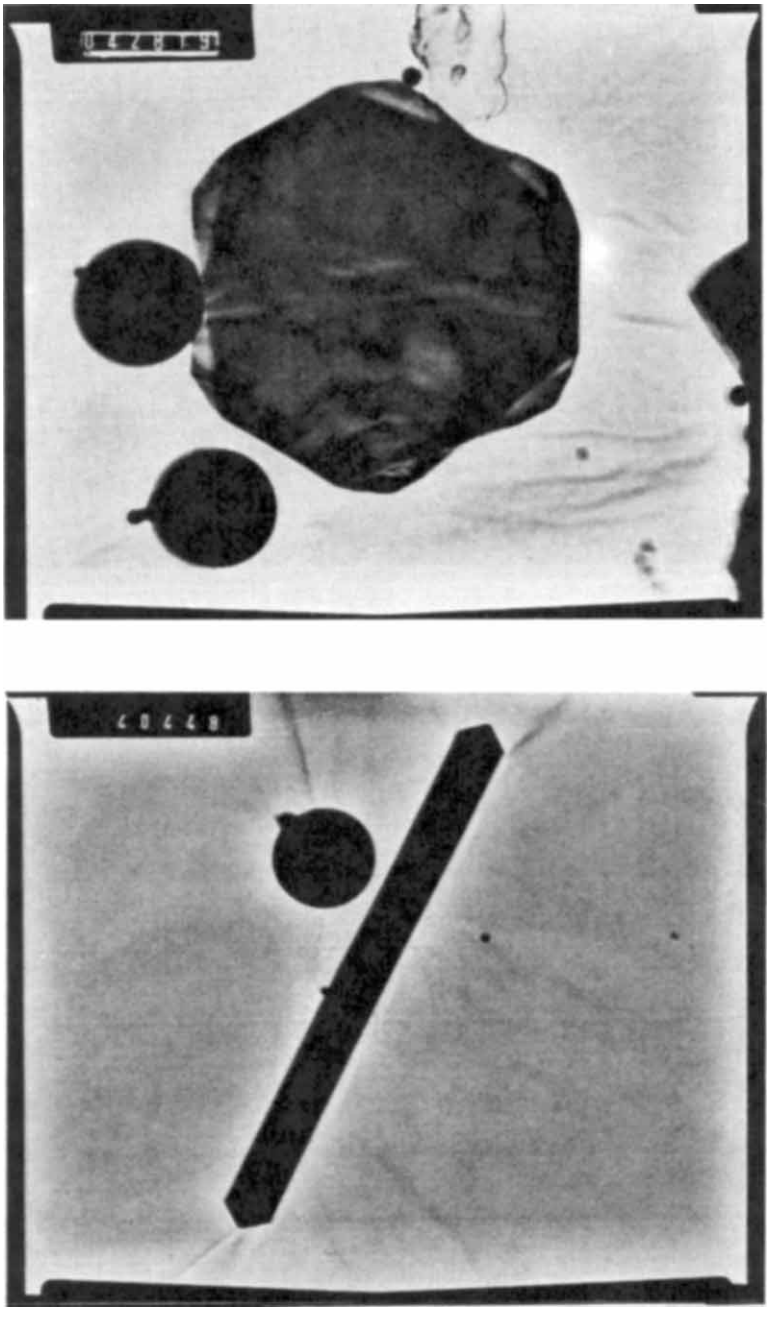

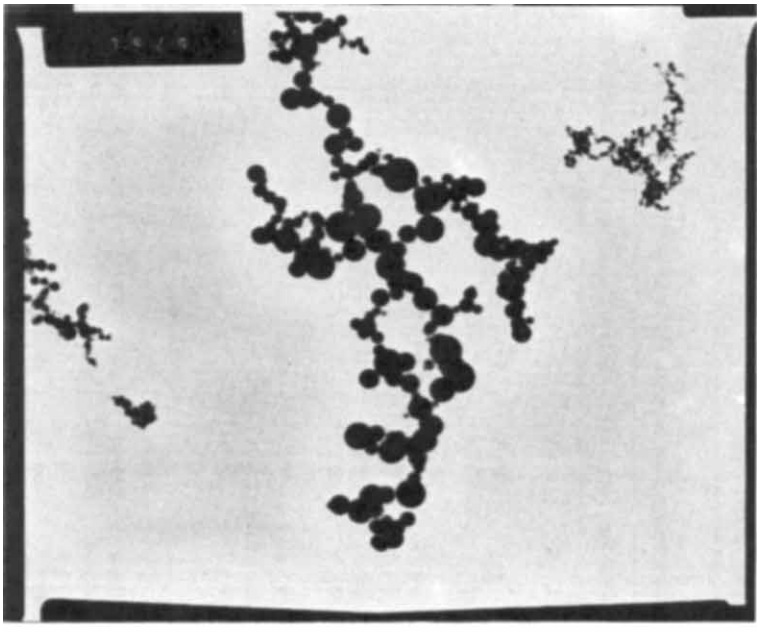

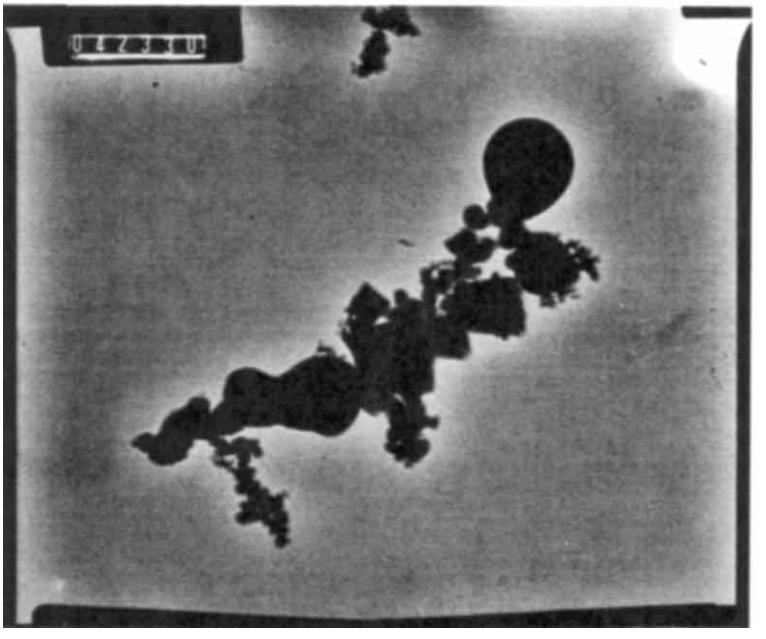

TABLE II

Relative abundance of Sb-containing particles in emission sources

Component	Sample	Impurities (%)						Mean projected diameter (μm)	distribution over impactor (% by number)				fraction of the total amount of particles (%)
		Pb	S	Fe	Zn	As	Cl		0.25–0.5 μm	0.5–1 μm	1–2 μm	2–4 μm	
Sb_2O_5 sphere, amorphous	blast furnace	19	14	—	—	—	—	0.21	—	—	—	—	2
	convertor (1)	5	10	2	—	—	—	0.40	22±2	68±6	10±1	—	79
	convertor (2)	1	9	1	—	—	—	0.33	22±2	70±6	8±1	—	70
	refinery oven	1	—	2	—	—	—	0.22	68±8	23±3	9±3	—	47
	stack 1 (1)	18	13	1	—	—	—	0.32	79±18	19±6	2.0±0.5	—	7
	stack 1 (2)	1	3	—	2	4	3	0.28	90±21	9±3	1.0±0.5	—	10
	stack 2 (1)	16	11	1	4	5	9	0.27	63±5	35±4	2.0±0.3	—	73
	stack 2 (2)	14	3	1	5	7	8	0.32	67±9	30±3	3±1	—	11
	stack 3	1	1	3	—	—	—	0.23	—	—	—	—	3
Sb_2O_5, aggregates	blast furnace	15	11	—	—	—	—	0.15	29±4	57±8	14±3	—	56
	stack 2 (1)	—	—	1	—	16	3	0.13	100±10	—	—	—	8
	stack 2 (2)	—	—	—	—	14	6	0.13	100±9	—	—	—	82
Sb_2O_3, senarmontite	blast furnace	—	—	1	—	—	—	2.0	—	—	—	—	1
	convertor (1)	—	1	1	—	—	—	1.0	~2	—	77±7	21±2	15
	convertor (2)	—	1	1	—	—	—	1.1	~1	40±4	55±6	3±1	15
	refinery oven	—	—	2	—	—	—	0.60	61±8	11±3	26±7	2±1	30
	stack 1 (1)	2	1	1	—	1	—	0.30	74±10	24±3	2.0±0.4	—	88[a]
	stack 1 (2)	3	3	—	—	—	—	0.45	87±9	8±2	5±1	—	74[a]
	stack 2 (1)	3	—	1	3	4	2	0.52	47±5	40±8	13±1	—	16
	stack 2 (2)	2	—	—	1	4	2	0.72	—	—	—	—	2
	stack 3	—	1	1	—	—	—	0.47	82±20	8±2	10±2	—	13

Sb_2O_3, aggregates	blast furnace	4	2	2	—	—	—	0.03	41±5	43±8	16±4	—	41
	convertor (2)	—	13	2	—	—	—	0.12	100±18	—	—	—	5
	stack 1 (1)	1	2	2	—	—	—	0.10	46±5	53±5	1.0±0.2	—	88[a]
	stack 1 (2)	—	—	2	—	—	—	0.14	99±10	1.0±0.3	—		74[a]
	stack 2 (1)	3	—	6	1	4	—	0.14	—	—	—	—	<1
	stack 2 (2)	3	—	7	1	4	—	0.15	—	—	—	—	4
	stack 3	—	1	2	—	—	—	0.15	82±9	16±2	2.0±0.4	—	82
$Sb_2O_3+Sb_2O_5$ aggr. senarmontite/ amorphous	refinery oven	—	—	4	—	—	—	0.03–0.3	71±9	19±4	9±4	~1	17
Sb_2O_3 senarmontite	convertor (1)	—	—	—	—	—	—	2.1	—	—	83±28	17±9	1
superstructure	convertor (2)	—	—	—	—	—	—	2.1	—	—	94±47	~6	1
	refinery oven	—	—	2	—	—	—	1.5	~24	16±12	56±25	~4	6
	stack 1 (1)	2	2	2	—	—	—	0.43	73±37	27±14	—	—	3
	stack 1 (2)	—	—	4	—	—	—	0.71	94±47	~4	~2	—	2
	stack 2 (1)	—	—	—	—	—	—	1.1	—	—	—	—	<1
	stack 2 (2)	—	—	1	—	—	—	1.1	—	—	—	—	<1
	stack 3	—	1	1	—	—	—	0.63	—	—	—	—	2
Sb_2O_3 valentinite	convertor (1)	—	—	—	—	—	—	2.9	~3	21±11	66±9	10±2	5
	convertor (2)	—	—	—	—	—	—	2.9	—	59±7	39±4	2±1	9
	refinery oven	—	—	1	—	—	—	3.7	—	—	—	—	<1
	stack 1 (1)	—	—	—	—	—	—	0.44	~73	~27	—	—	2
	stack 1 (2)	—	—	—	—	—	—	1.3	90±30	4±2	6±2	—	6
	stack 2 (1)	—	—	2	—	1	—	2.1	—	—	—	—	<1
	stack 2 (2)	—	—	1	—	1	—	2.1	—	—	—	—	<1
Sb_2O_3 transparent senarmonite	stack 1 (2)	2	2	—	—	—	—	0.81	95±28	3±1	2±1	—	8
	stack 2 (1)	3	2	—	—	4	—	0.95	47±24	49±37	~4	—	3
	stack 2 (2)	3	2	—	—	4	—	0.95	—	—	—	—	1

[a]Sum of single crystals and aggregates.

components were observed: Pb-based crystals with a high sulfur concentration and Pb-containing transparent spheres. Fly ash particles were also observed. They are easily distinguishable through their spherical appearance. X-ray emission spectra showed either an alumino-silicate or an iron matrix.

Study of the emission

Table II gives a summary of characteristic results for the different fugitive sources and stack emissions. In addition to the 4 distinct Sb-containing particle types discussed so far, 4 other morphologically and chemically identifiable particles are separately listed, namely aggregates of Sb_2O_5 particles, aggregates of senarmontite, transparent senarmontite and amorphous Sb_2O_5/Sb_2O_3 aggregates (Fig. 2f). Column 3 summarises the impurities detected. Results are mean values for the analysis of at least 20 particles and are semiquantitative with relative standard deviations of at least 30%. Column 4 shows the mean projected diameter for the measurement of at least 20 particles. The projected diameter according to Ledbetter[9] is the diameter of a circle with the same surface as the particle as seen in the position of maximum stability. Observations of particles with the electron miscroscope always indicated that particles are present on the support foil with this orientation. The relative importance of each of the components on 4 of the impactor stages as a number of particles (not mass) is summarised in column 5, whereas column 6 lists the relative abundance of each component in the different sources. For the latter two columns at least 200 particles were identified and used on every stage of the impactor.

Several of the emission sources were sampled repetitively. In general Sb-containing particulates have the same general characteristics (purity, abundance, projected diameter, repartition over the impactor stages). Table III gives a summary of triplicate data for one of the stack emissions.

The results for 2 typical samples obtained in the gas cleaning installation are summarised in Table IV. The material was ultrasonically treated for 1 h before sample preparation and measurement. Even then, the components remained considerably coagulated. Moreover, the surface of most of the particles was partly covered with small senarmontite crystals of $\sim 0.1\,\mu m$ projected diameter. These were not included in the compilation of Table IV.

It is readily apparent from Tables II and IV that the impurity content of the particles are potential source indicators for particles derived from different stages of the production process. The concentration of the impurities in the Sb_2O_5 particles decreases according to the sequence:

TABLE 3

Triplicate analysis in stack emission.

Component	Average projected diameter (μm)	Fraction of total (%)
Sb_2O_5 (amorphous spheres)	0.24	3
	0.21	4
	0.25	1
Sb_2O_3 (senarmontite)	0.44	13
	0.50	9
	0.59	11
Sb_2O_3 (senarmontite aggregates)	0.15	82
	0.15	85
	0.19	87
Sb_2O_3 (senarmontite superstructure)	0.71	2
	0.55	2
	0.92	1

TABLE 4

Antimony-containing particles in particulate material collected in gas cleaning equipment.

Component	Source	Concentration (%) Pb	S	Fe	Zn	As	Cl	Mean projected diameter (μm)	Fraction of the total % (by number)
Sb_2O_5 sphere, amorphous	convertor	14	5	3	—	—	—	0.62	10 ± 3
	refinery oven	1	5	—	4	7	7	0.60	11 ± 2
Sb_2O_3 senarmontite	convertor	1	1	2	—	—	—	1.3	88 ± 7
	refinery oven	—	—	—	—	3	—	1.3	77 ± 6
Sb_2O_3 senarmontite superstructure	convertor	—	—	2	—	—	—	1.3	~1
	refinery oven	—	—	—	—	—	—	1.4	$<<1$
Sb_2O_3 valentinite	convertor	1	1	1	—	—	—	2.4	~1
	refinery oven	1	3	1	1	1	—	3.0	3 ± 2
Sb_2O_3 transparent senarmontite	refinery oven	2	1	—	1	2	—	1.6	9 ± 2

blast furnace, convertor and refinery oven. For the blast furnace the lead concentration is of the order of 15% or higher in the fugitive emissions, the stack emissions and the filter bag material. For convertor sample 2 the impurity is lower than in sample 1 because of the purer starting product

used. The stack emissions of the refinery ovens contain a distinct Zn, Cl and As concentration.

Certain crystallographic varieties of the antimony oxide occur specifically in certain emissions. Valentinite and the superstructure of senarmontite are only present in the emissions of the refinery ovens, or convertors, never in the emissions from a blast furnace. Transparent senarmontite can be observed in the material emitted from the stacks only and originates in refinery oven emissions.

The projected diameters and the distribution over the impactor stages differs considerably from one type of emission to the other for morphologically and/or crystallographically identical particles. Sb_2O_5 particles from fugitive sources are much more abundant on stage 5 when they originate in a refinery oven, those emitted by convertors are more abundant on stage 4. Also, in general the size of particles emitted in the low altitude sources is higher than those emitted in the stacks. This is obviously due to the fact that the gas cleaning installations preferentially collect the largest size fraction. Filter bag material has indeed a larger projected diameter ($\sim 1.5\ \mu m$) compared to that of the stacks ($\sim 0.5\ \mu m$).

The following particles are typical for given emissions:

—valentinite and the superstructure of senarmontite are specifically produced in the convertors and refinery ovens;
—transparent senarmontite is observed only in the particulate material emitted through the stacks by a refinery oven;
—aggregates of Sb_2O_5 which contain a high lead concentration are typical for blast furnace fugitive or stack emissions;
—Zn, Cl and As containing Sb_2O_5 particles are indicators for stack emissions of a refinery oven;
—lead containing Sb_2O_5 single spheres were abundant for convertor emission (fugitive or stack), at least if they were not accompnaied by Sb_2O_5-aggregates. Otherwise they may also result from a blast furnace;
—pure Sb_2O_5 spheres are indicative for the fugitive emissions of a refinery oven.

The fly-ash emissions are too unspecific for the operation of the factory to be of any use as an indicator.

Measurements in the sampling network

Measurements of particulate matter at the sampling locations A, B and C of Fig. 1 indicate the prominence of the Sb- and to a lesser degree the Pb-containing particles derived from the emission sources in the factory. No significant changes were noted between the morphological and size

characteristics at the emission sites and in the field. Table V summarizes data measured for Sb_2O_5 spheres with negligible impurity content originating as a fugitive emission for a refinery oven. The distribution over the cascade impactor stages is consistent with measurements at the emission. The average projected diameter of 0.18 μm is in agreement with that measured at the refinery oven. Other evidence points to the same conclusion. One major difference is however, apparent,: the particles obtained in the sampling network acquired a sulphur impurity which most probably results from the adsorption of water-soluble sulphates.

TABLE V

Particle size distributions over the collector stages for Sb_2O_5 spheres in sampling network (% by particle number).

	Sampling location								
	A			B			C		
Sample	0.25–0.5 μm	0.5–1 μm	1–2 μm	0.25–0.5 μm	0.5–1 μm	1–2 μm	0.25–0.5 μm	0.5–1 μm	1–2 μm
1	81±10	13±1	6±1	82±10	15±2	3±1	81±10	16±3	3±1
2	77±9	14±2	9±1	73±7	17±2	10±2	73±9	22±3	5±2

Table VI shows a number of components which originate in the factory and which are easily measurable. Some particulates are readily detectable in samples obtained at locations B and C but are absent at location A: impure Sb_2O_5 spheres, transparent senarmontite, Pb particles and fly-ash particles. Roughly, Sb particles and Pb particles are responsible for 45 and 10% of the total number of particles at locations B and C.

Earlier evidence obtained by bulk analysis in the sampling network[10] already indicated that within ±1500 m, i.e. at location C, fugitive emissions dominate over the emission of the high altitude sources. Also, for the most frequently occurring atmospheric stability classes, a maximum stack emission contribution was calculated by Bultynck.[11] It invariably occurs at distances of 400 to 2000 m from the stacks, i.e. at a larger distance than location A. The results of Table VI agree with all this information.

It was attempted to study quantitatively the atmospheric impact of the different emission sources at the 3 locations in the sampling network using the previously mentioned specific tracers. Table VII gives the results for 2 samples taking during short sampling times which correspond with

TABLE 6

Antimony-containing particles in field samples

Identification	Found in sampling location		Concentration of impurities (atom %)	mean projected diameter (μm)	distribution over the impactor (%)		
	sample 1	sample 2			0.25–0.5 μm	0.5–1 μm	1–2 μm
Sb_2O_5 sphere, amorphous	A, B, C	A, B, C	2% Pb	0.18	81 ± 10	13 ± 1	6 ± 1
Sb_2O_5 sphere, amorphous	B, C	C	2% Zn, 7% As, 4% Cl	0.30	~71	~21	~8
Sb_2O_5 sphere, amorphous	B, C	B, C	25% Pb	0.35	~83	~ 8	~9
Sb_2O_3, senarmontite	A, B, C	A, B, C	<1%	0.37	51 ± 8	19 ± 2	30 ± 4
$Sb_2O_3 + Sb_2O_5$ aggregates senarmontite + amorphous	A, B, C	A, B, C	<1%	0.03–0.3	72 ± 11	23 ± 3	5 ± 2
Sb_2O_3, superstructure of senarmontite	A, B, C	A, B, C	<1%	0.52	47 ± 35	31 ± 6	22 ± 9
Sb_2O_3, valentinite	A, B, C	A, B, C	<1%	1.9	—	—	—
Sb_2O_3, transparent senarmontite	B, C	C	<1%	1.2	—	—	—

specific working conditions within the factory: no blast furnaces were active and no convertors were loaded during sampling.

The analysis of the particulates proves the absence of Sb_2O_5 aggregates which are characteristic for blast furnace emission. The total concentration of particles at the different sites differs strongly from the Sb gradients measured by bulk analytical methods for the total suspended particulate material, which show an exponential decrease with distance with roughly a drop by a factor 2 every 500 m.[10] This illustrates the strongly discontinuous character of the emissions. For other samples taken at location A, the particle concentration increases up to 1.6×10^9 particles m^{-3} for high fugitive emission. By straightforward calculations using the different particle fractions the relative abundances of the three active emissions shown in Table VII were calculated. It is difficult to obtain any safe indication of the reliability of these results, but we can assume from the reproducibility of the particle measurements that inaccuracies are below 30%.

TABLE 7
Source tracing of particulate matter at field locations.

Sample	Sampling location	Particles/m^3 ($\times 10^{-6}$)	Relative abundance (% in number of particles)		
			fugitive emission	stack emission	
			refinery oven	refinery oven	convertor
1	A	190	100	—	—
	B	67	93	3	4
	C	32	66	6	28
2	A	3.1	100	—	—
	B	76	97	—	3
	C	18	72	6	22

CONCLUSIONS

A detailed investigation of the individual antimony-containing particulates by transmission electron microscopy in the various fugitive and stack emission sources of an antimony (and lead) refining plant, allows source partitioning of the individual sources up to 1.5 km away downwind from the sources. It confirms other evidence that fugitive emissions are far more important than stack emissions and that any further pollution abatement strategies at the site hence have to be centered on the reduction of the fugitive sources.

Also, it appears that except for the formation of a mantle of sulphates, the particles do not undergo systematic changes in morphology, chemical composition and size.

The procedure applied is very time consuming: the full study required about 1 man-year, and requires costly instrumentation. Nevertheless it provides a direct and straightforward quantitative estimate of sources even within a single industrial complex which other macroscopical methods could not provide.

Acknowledgments

This work was carried out in the framework of the National Research and Development Program on Environment and Concerted Research Action 80–85/10 of the Interministerial Commission for Science Policy, Belgium. Thanks are due to P. Geladi, G. Van Tendeloo and D. F. S. Natusch for valuable discussions.

References

1. P. Bloch, P. Geladi, F. Adams, G. Van Tendeloo and J. Van Landuyt, *J. Trace and Microprobe Techniques*, in press.
2. R. Mitchell and J. Pilcher, *Ind. Eng. Chem.* **51,** 1039–1042 (1959).
3. Luchtverontreiniging door een metallurgisch bedrijf. Report of the National R & D program Environment–Air Belgium, Ed. Programmatie van het Wetenschapsbeleid, Brussels, 1982.
4. P. Van Espen, H. Nullens and F. Adams, *Nucl. Instrum. Methods* **142,** 243–250 (1977).
5. P. Van Espen, H. Nullens and F. Adams, *Nucl. Instum. Methods* **145,** 579–582 (1977).
6. J. C. Russ, *X-ray spectrometry* **1,** 119–123 (1972).
7. J. Van Landuyt, G. A. Wiegers and S. Amelinckx, *Phys. Stat. Sol. A.* **46,** 479–492 (1978).
8. R. De Ridder, D. Van Dijk and S. Amelinckx, *Phys. Stat. Sol.* (*a*) **50,** K67–K71 (1978).
9. J. D. Ledbetter, *Air Pollution, Part A, Analysis* (Marcel Dekker Inc., New York, 1972).
10. R. Dams, B. Vanderborght and F. Adams, *Environmental Technology Letters* **3,** 337–344 (1982).
11. H. Bultynck and L. Malet, *Tellus* **24,** 455–472 (1972).